



**HAL**  
open science

## Hydraulic criteria for internal erosion in cohesive soils

Stéphane Bonelli, Didier Marot, Fabien Ternat, Nadia Benahmed

► **To cite this version:**

Stéphane Bonelli, Didier Marot, Fabien Ternat, Nadia Benahmed. Hydraulic criteria for internal erosion in cohesive soils. Annual meeting of the European Working Group on internal erosion in embankment dams, Apr 2007, Aix-les-Bains, France. hal-01008261

**HAL Id: hal-01008261**

**<https://hal.science/hal-01008261>**

Submitted on 12 Feb 2024

**HAL** is a multi-disciplinary open access archive for the deposit and dissemination of scientific research documents, whether they are published or not. The documents may come from teaching and research institutions in France or abroad, or from public or private research centers.

L'archive ouverte pluridisciplinaire **HAL**, est destinée au dépôt et à la diffusion de documents scientifiques de niveau recherche, publiés ou non, émanant des établissements d'enseignement et de recherche français ou étrangers, des laboratoires publics ou privés.

# Criteria of Erosion for Cohesive Soils

S. Bonelli, D. Marot, F. Ternat, N. Benahmed

## Abstract

This paper focus on three types of erosion: the suffusion, the backward erosion, and the piping erosion processes. A new triaxial device to quantifying suffusion and backward erosion, and a new model for interpreting the Hole Erosion Test, are presented. It is recommended to use these erosion tests in order to evaluate the erosion parameters on any sample of cohesive soil from a site.

## 1 Introduction

Erosion can only develop if two vital conditions are met: particles must be torn off and must be transported. Four types of erosion process, internal to the work, have been identified [Fell and Fry, 2007]: 1) suffusion, which affects the soil structure, 2) evolution of defects in the soil matrix (holes, cracks), 3) backward erosion, 4) contact erosion between two soils.

After exposing a new approach concerning the critical erosion shear stress for cohesive soil, the present paper presents some recent results concerning types 1), 2) and 3): the suffusion and backward erosion processes, internal to the soil, and the piping erosion process, external to the soil and internal to the work.

## 2 Critical Erosion Shear Stress for Cohesive Particles

Basically, the critical erosion shear stress of cohesive sediments depends on the granulometry (i.e. particle size and shape) and cohesive particle content whose diameter is finer than  $2\mu\text{m}$  [Graf, 1984]. A strong dependence on the consolidation degree of the water/sediment mixture has also been highlighted [Mitchener, 1996]. This consolidation degree can be related to various experimental measurements such as porosity or water content measurements [Sunborg, 1956; Migniot, 1968]. The Atterberg limits are also useful, as featured on Table.1, but specific interpretation of this parameter is required to relate it to mechanical properties of the sediment. Particle whose diameter is smaller than  $2\mu\text{m}$  are suggested to interact by the mean of the Van der Waals force. Its expression between two spherical particles of diameters  $d_1$  and  $d_2$ , separated with the distance  $d_i$ , [Israelachvili, 1985] can be written in the following way:

$$F_H = A_H/12 * d_1 * d_2 / (d_1 + d_2) / d_i^2 \quad (1)$$

Recent work has tried to evaluate this particular cohesion force [Ternat, 2007]. The main difficulty remains in the determination of the interparticle distance  $d_i$ , which has been linked to the porosity  $n$ , considering a crystalline modelling of the particle network. This modelling provides, on the one hand, the expected link between interparticle distance and the porosity, but on the other hand, it also provides a multiplicative factor  $C_i$ , called coordination, that is used to account for multiple interactions. For instance, here is the expression of the interparticle distance between two same size particles:

$$d_i = d \left( \frac{[(n_{\max} - n_{\min}) / (n_{\max} - n)]^{1/3} - 1}{C_i} \right) \quad (2)$$

where  $n_{\max}$  and  $n_{\min}$  are respectively the maximum and the minimum values of the porosity, corresponding respectively to the most compacted and the loosest states of the sediment,  $n$  is the local porosity. The coordination factor is considered to vary like the cube of the ratio between the two particle sizes:

$$C_1 \sim (d_1/d_2)^3 \quad (3)$$

Finally, the resulting cohesion force becomes:

$$F_C = F_H * C_1 \quad (4)$$

Once determined, the cohesion force is included into the usual force balance considered to assess the critical shear stress [Dade, 1992; Graf, 1984; Wiberg, 1987]. The erosion criterion is expressed in the following form:

$$F_D = \tan \Phi (F_W - F_L + F_C) \quad (5)$$

Where  $\Phi$  is the internal angle,  $F_D$  is the drag force of the flow,  $F_L$  is the lift force of the flow,  $F_W$  the buoyant weight of the particle and  $F_C$  the cohesion force. The drag force must account for the granulometry of the eroded surface, which is achieved in the drag coefficient [Graf, 1984]. The lift force is also described and can be accurately determined [Yalin, 1977; Saffman, 1965]. Note that hydrodynamic forces are valid in the viscous domain ( $Re^* < 1$ ), determining thus the validity domain of the present model. The granulometry of the eroded surface is accounted by means of the  $\alpha$  coefficient, characterizing the relative position of the particle related to the sediment/water interface. There is little controversy concerning the buoyant weight of the particle, which can be obtained by the product of the particle volume with its specific weight. All these contributions are adjusted with shape factors, related to each force:  $k_D$  for the drag force,  $k_L$  for the lift force,  $k_W$  for the buoyant weight. Gathering all those information leads to an expression of the critical shear stress for the erosion of a spherical cohesive particle, in terms of dimensionless Shields parameter  $\tau^*$  in function of the particle Reynolds number  $Re^*$ :

$$\tau^* = \frac{k_W \frac{\tan \Phi}{\alpha k_D}}{a + \frac{k_L}{k_D} \tan \Phi . Re^* + \frac{3 \cdot \alpha \cdot \alpha}{16} . Re^{*2}} \left( 1 + \frac{F_C}{F_W} \right) \quad (6)$$

where  $a$  is a constant of the drag coefficient. This expression features the rule of the cohesion function ( $1 + F_C/F_W$ ) that increases the value of the erosion threshold since  $F_C$  becomes comparable to  $F_W$ . Let's note that the determination of the erosion threshold does not present any difficulty to be solved when  $F_C$  is null, but a numerical resolution must be done when not.

To illustrate these approaches, here are examples of possible results. Firstly, it is interesting to have a look over the cohesion function that features a critical diameter smaller than a few microns, where cohesion between two particles becomes efficient (**Figure 1**). When multiple interactions are accounted for, cohesion affects all the particle range present in the granulometry, revealing a kind of cementation of coarse particles by fine ones (**Figure 2**).

It is then possible to obtain the critical erosion velocity  $u^*$  (m/s), defined by  $\tau^* = \rho_w \cdot u^{*2}$  in function of the particle diameter  $d$  (**Figure 3**).

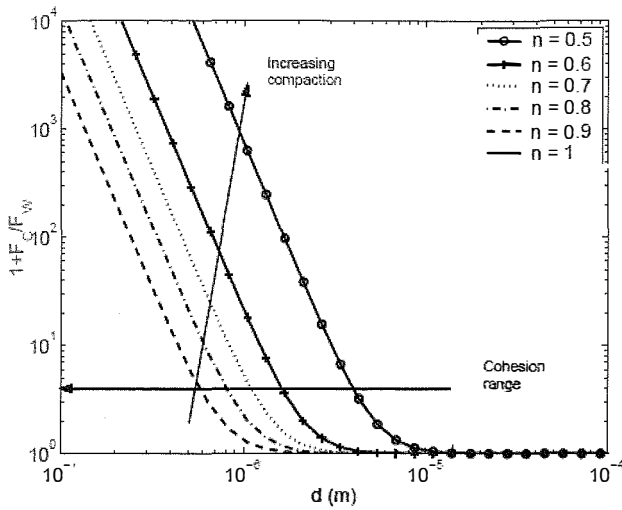


**Figure 1:** Evolution of the cohesion function  $1 + F_C/F_W$  vs. particle diameter  $d$  for different porosity values.

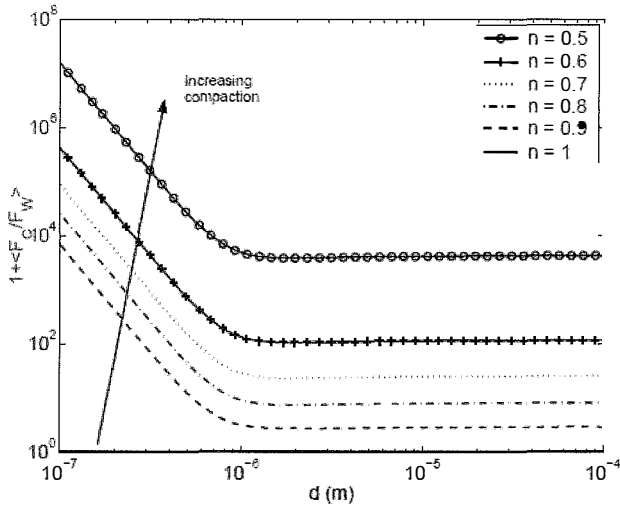


**Figure 2:** Evolution of the cohesion function  $1 + F_C/F_W^2$  vs. particle diameter  $d$  for different porosity values.

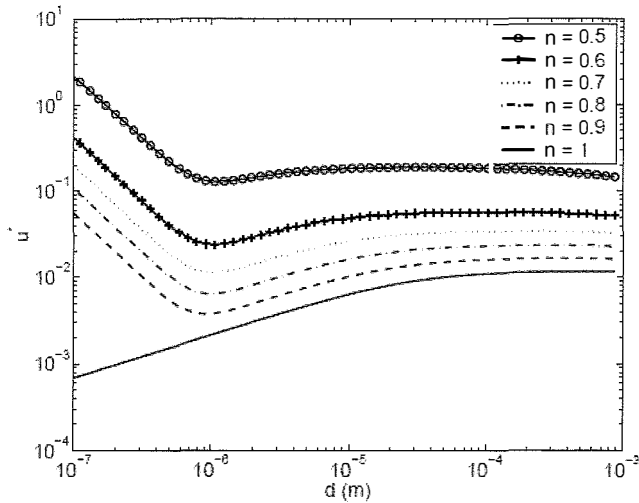


**Figure 3:** Evolution of the critical erosion velocity  $u^*$  vs. particle diameter  $d$  (m) for different porosity values.

All the parameters values required for the application of the presented modelling are given on Table 2.

This section reveals a first simple approach for assessing the critical erosion threshold of cohesive sediments. It is deduced from a force balance that includes the cohesion force, attributed to the presence of clay particles. This force, supposed to be the surface Van der Waals interaction, is directly dependent on the compaction degree and the particle size. The present model integrates all these declarations and introduces the porosity as a main parameter. Results reproduce well the main declarations of the literature: cohesion force appears to come from the presence of clay particles, and thanks to the coordination number, coarse particles are also affected. The usual critical shear stress magnitude is assessed in good agreement with the literature.

This model is interesting because of its simple parameterization by means of granulometry and porosity. The geometric factor including the unknown coordination appears also as a parameter, but whose value includes measurement and modelling errors. This original work results from the gathering of many models, which may be ameliorated. At the moment and to our knowledge, no modelling pretends to assess the coordination of such a wide range granulometric mixture. Moreover, cohesion is here attributed to the presence of clay particles, and is reduced to one of its components, the Van der Waals force. Other forces should also be incorporated to refine the results, such as double layer or chemical interactions.

Tab. 2: Numerical values of the parameters for the erosion threshold resolution

| Symbol    | Value             | Units              |
|-----------|-------------------|--------------------|
| $\rho_s$  | 2650              | kg.m <sup>-3</sup> |
| $\rho_w$  | 1000              | kg.m <sup>-3</sup> |
| G         | 10                | m.s <sup>-2</sup>  |
| $\Phi$    | 52,5              | °                  |
| $A_H$     | 10 <sup>-20</sup> | J                  |
| $\alpha$  | 0,16              | [-]                |
| A         | 37,49             | [-]                |
| $k_D$     | 0,4               | [-]                |
| $k_L$     | 30                | [-]                |
| $k_W$     | 1                 | [-]                |
| $n_{max}$ | 1                 | [-]                |
| $n_{min}$ | 1- /6             | [-]                |

### 3 Internal Erosion in Cohesive Soils without Crack

The two main phenomena responsible for erosion of particles in uncracked soils are backward erosion and suffusion. In backward erosion particles are detached from the downstream surface by the outward seepage. The suffusion process is similar but the coarse particles form a matrix and erosion is only of the finer particles in the pore space between the larger particles.

#### 3.1 Criteria

Soil structure can be analyzed into two groups: a primary structure and a secondary structure [Kenney and Lau, 1985]. The primary structure consists of grains, which are in contact with each other and provide primary resistance to erosion, compressibility and shear strength. If these grains are eroded there are changes to the soil resistance and this may cause collapses. The secondary structure, on the other hand, is composed of grains, which are in the spaces between the primary grains and, which may be displaced under the action of mechanical (vibration) or hydraulic (flow) stresses.

On the assumption that bigger grains can hinder the erosion of smaller grains, Kenney and Lau [1985] have developed a method for assessing whether soils are internally unstable based on the shape of the coarse or the fine low-content grading curve. However, the method does not apply to clay soils.

In order to characterize the initiation of internal erosion for cohesive soils, Reddi et al. [2000] have developed an expression of the hydraulic shear stress  $\tau$ :

$$\tau = \frac{\Delta p}{L} \sqrt{\frac{2 \lambda}{n}}, \quad \lambda = \frac{\eta_w k}{\gamma_w}, \quad (7)$$

where  $\Delta p/L$  is the average pressure gradient,  $\lambda$  is the intrinsic permeability,  $n$  is the porosity,  $k$  is the engineering hydraulic permeability,  $\eta_w$  and  $\gamma_w$  are the water viscosity, and specific weight, respectively.

### 3.2 The Triaxial Device

The developed experimental device can be used to study the initiation of suffusion and backward erosion for sandy-clay samples (**Figure 4**).

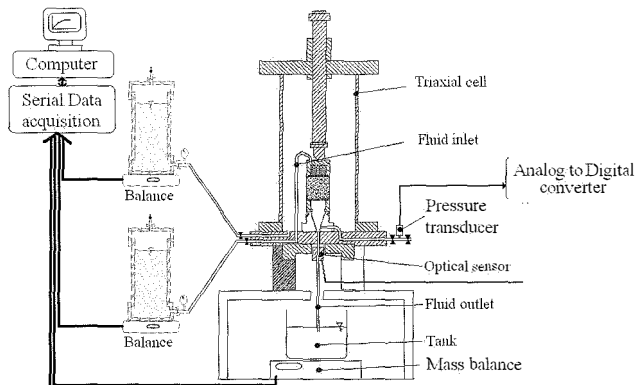


**Figure 4:** Schematic representation of the experimental triaxial cell equipped with the two controllers, effluent weight measurement and optical sensor mechanism (GeM).

The device placed in a temperature-controlled chamber ( $20 \pm 0.5 \text{ }^\circ\text{C}$ ) consists of three modified triaxial cells. These cells have been modified to let the flow come through up to the core of the sample. So as to avoid all unwanted disturbances on the samples, saturation, consolidation, hydraulic and mechanical test stages are carried out inside the same cell without deconfining the samples. The carrying out of long-lasting tests is possible thanks to the automation of both the monitoring and the data acquisition. The use of three cells simultaneously makes it possible to reduce the duration of the test program.

The detection of erosion in the effluent is performed using optical aids and by weighing the amount of grains in the eroding fluid. The internal erosion critical gradient can be assessed from the effluent instantaneous optical analysis. In order to address internal erosion development, injection volume flow rates and obtained mass flow measurements are compared. A detailed description is given by Bendahmane et al. [2006].

### 3.3 Results

The material used is a washed Loire sand (grain density: 26 kN/m<sup>3</sup>) with a grain size distribution within the range 80µm-1mm ( $d_{50} = 440\mu\text{m}$ , uniformity coefficient: 3.125). The clay consists of kaolinite, with liquidity and plasticity limits are 55% and 22%, respectively.

In order to improve understanding of the phenomena, a distinction is made between the tests during which only clay particle migration is initiated, and the tests during which the transport of both clay particles and sand grains is observed. Maximum erosion rates per sample sections are preferred to some cumulative eroded mass information because the erosion rate here reaches its maximum value very quickly, which therefore means that it does not depend on the test duration.

#### 3.3.1 Clay Erosion

From the beginning of the test, the mass flow increases until reaching a maximum value,  $q_{s\text{max}}$ . It then decreases asymptotically toward zero. The permeability remains constant when no erosion occurs, but it decreases where erosion has been initiated. The erosion occurring within the clay fraction does not affect the size analysis nor the volume of the samples significantly. Consequently, according to the previously defined terminology, this phenomenon, characterized by some diffuse mass losses can be called suffusion.

The impact of three different parameters on the initiation of suffusion has been examined:

- kaolinite content: 5, 10, 20 and 30%;
- hydraulic gradient ranging between 5 and 160 m/m;
- confining pressure  $\sigma_3$ : 100, 150, 200 and 250 kPa.

The range of hydraulic gradient was chosen relatively large to include the possible reduction of flow path in an earth structure by backward erosion phenomena. In this case, the local gradient can be much higher than the global one. The rate of suffusion increases according to the hydraulic gradient as follows:

$$q_{s\text{max}} = 16.6 (10^{0.02(i-5)} - 1) \quad (8)$$

where  $i = \Delta p / (\gamma_w L)$  is the hydraulic gradient.

Obtained results show that, depending on the hydraulic gradient, the erosion of the soils studied decreases as a function of the clay content according to:

$$\text{for } i = 20\text{m/m} : q_{s\text{max}} = -0.06 \% \text{clay} + 1.28 \quad (9)$$

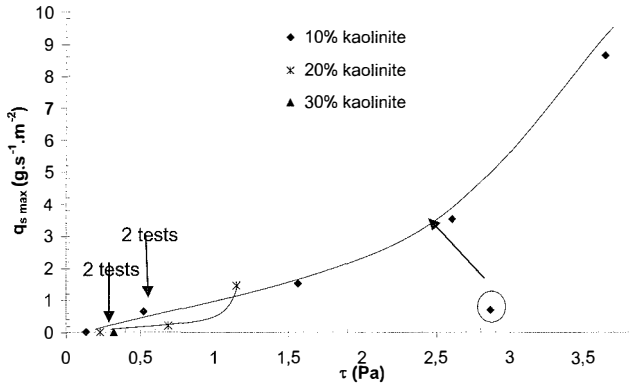
$$\text{for } i = 60\text{m/m} : q_{s\text{max}} = -0.13 \% \text{clay} + 2.85 \quad (10)$$

$$\text{for } i = 100\text{m/m} : q_{s\text{max}} = -0.17 \% \text{clay} + 5.15 \quad (11)$$

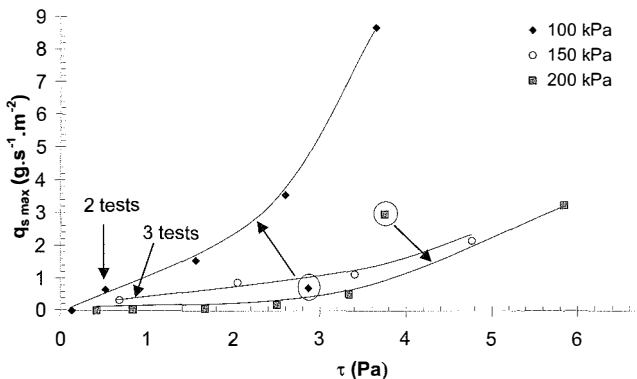
In a general way, the erosion rate doubles when the clay content changes from 20 to 10%.

Figure 5 represents the evolution of the maximum erosion rate according to the hydraulic shear stress Eq. (7) for  $\sigma_3 = 100$  kPa.

The initial porosity depending on the consolidation, studying the effects of the confining pressure is essential. For sand specimens subjected to oedometer confinement conditions, Papamichos et al. [2001] observe that the maximum erosion rate growth according to the axial pressure applied is destabilizing. The present tests conducted under isotropic confinement with a 20 m/m hydraulic gradient and a 10 % clay content, reveal some opposite results (**Figure 6**).



**Figure 5:** Maximum erosion rate v.s. hydraulic shear stress according to clay content ( $\sigma_3 = 100$  kPa).



**Figure 6:** Maximum erosion rate v.s. hydraulic shear stress according to confining pressure (10% clay content)

Depending on the hydraulic gradient value, the linear decrease of the maximum erosion rate according to the confining pressure as follows:

$$\text{for } i = 20 \text{ m/m : } q_{s \max} = -0.006\sigma_3 + 1.256 \quad (11)$$

$$\text{for } i = 60 \text{ m/m : } q_{s \max} = -0.013\sigma_3 + 2.877 \quad (12)$$

To obtain the same maximum erosion rate, the hydraulic shear stress has to increase as a function of the confining pressure.

This approach makes it possible to identify the minimum stress levels, which depend on both clay contents and confining pressures and below which suffusion will not occur for the soils tested. For example, we obtained for  $\sigma_3=100$  kPa

$\tau_{cr} = 0.13$  Pa with a 10 % clay content;

$\tau_{cr} = 0.23$  Pa with a 20 % clay content;

$\tau_{cr} = 0.32$  Pa with a 30 % clay content.

For  $\sigma_3= 200$  kPa and a 10 % clay content,  $\tau_{cr}$  is approximately 0.42 Pa.

These values are several orders of magnitude greater than those in the case of surface erosion experiments, referring notably to the results from tests done in rotating cylinders [Arulanandan and Perry, 1983] or HET [Reddi et al., 2000]. However these values are four times smaller than those from Reddi et al. [2000]'s measurements in the case of internal erosion experiments. The direct application of our results and Reddi et al. [2000]'s seems to be difficult for the moment. The result difference observed between the samples tested here, and the Ottawa sand + kaolinite mixtures tested by Reddi et al. [2000] can be accounted for by many reasons. First the characteristics of the filter can either be open or be a porous stone may be responsible for these differences. The sand itself could also play a role, as grain sizes and grain angularities were different in our and their experiments.

The result difference observed between the samples tested here and Papamichos et al. [2001]'s specimens can be accounted for by many reasons: the characteristics of the pressure first, which can be isotropic or axial, of the samples, which can be made of a sandy-clay mixture or composed of sand only, then of the phenomena examined which are interpreted to be suffusion or backward erosion, and the sand grain angularity.

### 3.3.2 Clay and Sand Erosion

Considering two samples, both with a 10 % clay content and consolidated at 150 kPa. The first sample subjected to the action of a hydraulic gradient of 60 m/m suffers some clay erosion, whose extent is measured using the optical sensor, which gives a clay eroded mass of 60 mg. The second sample, on the other hand, subjected to a 140 m/m hydraulic gradient, gives a weighed eroded mass (clay and sand) of approximately 40 g.

The quantity of effluents achieved here (17% of the sample initial volume) produces a substantial volume variation within the sample, which finally collapses revealing then a significant change in the erosion mechanisms. Clay and sand particles are discharged from the soil downstream and along the upstream line through a backward erosion mechanism occurring within the sample.

Figure 7 shows the effects of the confining pressure on the maximum erosion rate (determined by weighing regarding sand erosion). This confirms that when the confining pressure rises, sand erosion within the samples tends to increase.

Backward erosion critical gradient values are very high, and, like suffusion, depend on both clay content and confinement stress. For clay contents higher than 10%, no backwards erosion effect is observed whereas, which a 10 % clay content, the backward erosion critical gradient is

90 m/m with  $\sigma_3 = 200$  kPa ;

100 m/m with  $\sigma_3 = 150$  kPa ;

140 m/m with  $\sigma_3 = 100$  kPa.

The backward erosion increase as a function of confining pressure confirms conclusions of Papamichos et al. [2001] achieved with specimens made of sand only.

This experimental study opens up many new research prospects to address the problem of suffusion and backward erosion processes while demonstrating the importance of confinement effects on internal erosion. As the relationships between internal erosion processes and geotechnical or chemical properties of the soils remain unknown, it is recommended to use this test in order to evaluate the suffusion parameters on any sample of cohesive soil from a site.

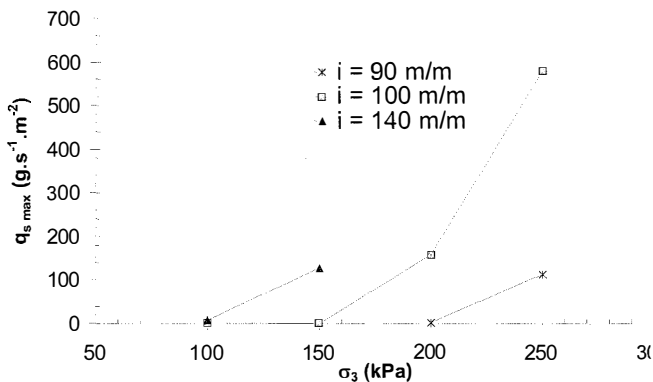


Figure 7: Maximum erosion rate v.s. confining pressure (10% clay content)

## 4. Piping Erosion in Cohesive Soils

Piping erosion is internal to the work, but external to the soil: this is a surface erosion. A large literature on surface erosion exists in the field of hydraulics and river engineering [Graf, 1984], [Yalin, 1977] and in the field of poromechanics and petroleum engineering [Papamichos et al., 2001]. In the field of geomechanics, several experimental methods have been developed for simulating the piping erosion process experimentally, with particular attention focussed on the hole erosion test. The experience acquired on more than 200 tests on several soils has confirmed what an excellent tool this test can be for quantifying the rate of piping erosion in a soil.

#### 4.1 Criteria

Piping occurs if  $P_0 > \tau_c$  where  $P_0$  is the initial tangential shear stress exerted by the piping flow on the soil, and  $\tau_c$  is the critical stress. The scaling law of radius time evolution is [Bonelli et al., 2006]

$$R(t) = R_0 \left[ \frac{\tau_c}{P_0} + \left( 1 - \frac{\tau_c}{P_0} \right) \exp\left( \frac{t}{t_{er}} \right) \right], \quad (13)$$

with

$$P_0 = \frac{R_0 \Delta p}{2L}, \quad t_{er} = \frac{\rho_d R_0}{C_e P_0},$$

where  $t_{er}$  is the characteristic time of piping erosion,  $R_0$  is the initial radius,  $\Delta p$  is the pressure drop,  $L$  is the hole length,  $\rho_d$  is the dry soil density, and  $C_e$  is the Fell coefficient of soil erosion. The later is similar to the Temple and Hanson [1994] coefficient of erosion  $k_d$ , as  $k_d = C_e / \rho_d$ . The Fell erosion index is  $I_e = -\log(C_e)$  ( $C_e$  given in s/m).

#### 4.2 Influence of Soil Properties

All test results - Temple and Hanson [1994] jet tests, Briaud EFA [2006] tests or Wan and Fell [2002] hole erosion tests - give a interesting relationship between the critical stress and the coefficient of erosion, or equivalently between the critical stress and the erosion rate index:  $I_e$  is proportional to  $\log(\tau_c)$ . The greater the critical stress, the greater the erosion rate index (the slower the erosion).

It is well known fact that different soils erode at different rate. Attempts were made to correlate erosion parameters - critical stress and coefficient of erosion - to common geotechnical or chemical soil properties in hope that simple equations could be developed for everyday use.

As a matter of fact, the erosion strength has been found to increase with: 1) the dry density of the soil, 2) the percent clay. This is illustrated by the following correlation [Temple and Hanson, 1994]:

$$I_e = 2 + 0.052 \left( \rho_d / \rho_w \right)^{3.1} (\%clay)^{0.406}. \quad (14)$$

However, for others parameters like the plasticity index, the liquid limit, the percent fines, the shear strength or the salinity, the situation is not clear. Due to the interdependence of these properties, however, it is clear that erosional strength of a soil cannot be represented accurately by the algebraic sum of the contribution of each of its properties. All attempts failed to reach a reasonable correlation coefficient value [Briaud, 2006]. It is strongly recommended carrying out hole erosion tests rather than using correlations [Wan and Fell, 2002].

#### 4.3 The Hole Erosion Test

The hole erosion test was designed to simulate piping flow erosion in a hole. This test is not new [Lefebvre et al., 1985]. An eroding fluid is driven through the soil sample to initiate erosion of the soil along a pre-formed hole (**Figure 8**).

The results of the test are given in terms of the flow rate versus time curve with a constant pressure drop. Therefore, the flow rate is used as an indirect measurement of the erosion rate. For further details about this test, see [Wan and Fell, 2002].

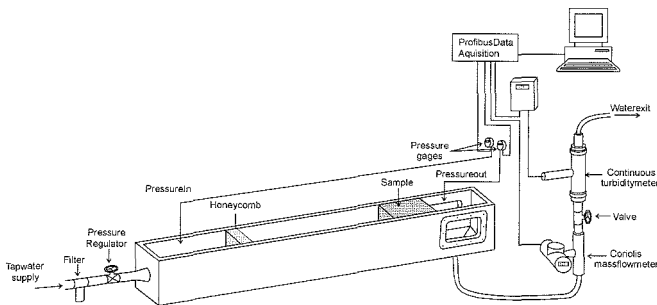


**Figure 8:** Schematic representation of the hole erosion test apparatus (Cemagref)

#### 4.4 Results

The scaling law is now compared with previously published data [Wan and Fell, 2002]. Analysis were performed in 18 tests, using 9 different soils (clay, sandy clay, clayey sand or silty sand). The initial radius and the length of the pipe were  $R_0=3$  mm and  $L=117$  mm. Table 1 contains particle size distribution, and critical stress and Fell erosion index.

Figure 9 gives the effect of erosion process as the flow rate in relation to time, and shows that the use of  $t_{er}$  leads to efficient dimensionless scaling. Without this scaling, multiple graphs would be necessary to provide clarity of presentation. Scaled radius are plotted as a function of the scaling time in Figure 10. Nearly all the data can be seen to fall on a single curve. This graph confirms the validity of the scaling law (13).

Therefore, it is recommended to use hole erosion tests and the scaling law in order to evaluate the piping erosion parameters on any sample of cohesive soil from a site.

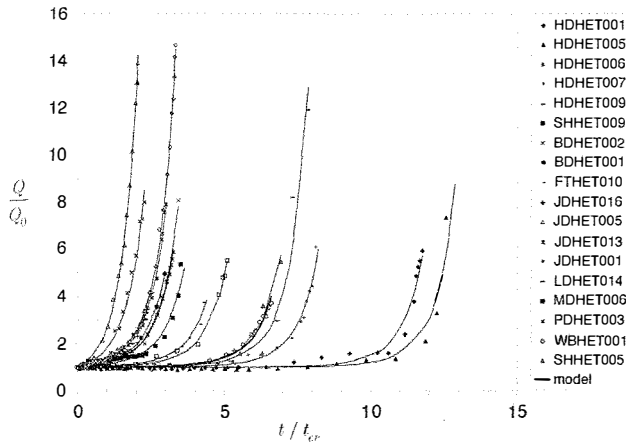


Figure 9: Hole Erosion Tests (symbols) versus scaling law (continuous lines). Dimensionless flow rate is shown as a function of dimensionless time.

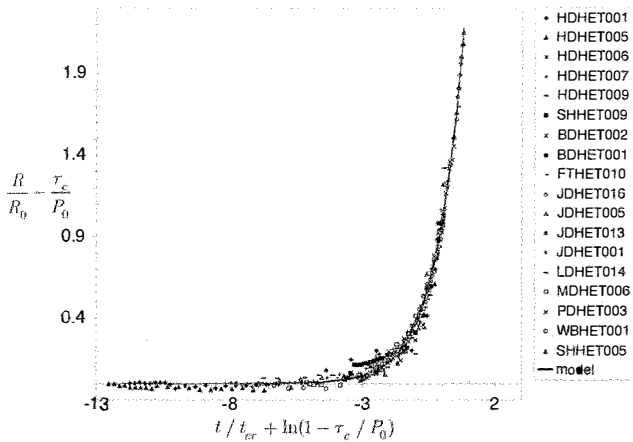


Figure 10: Hole Erosion Tests (symbols) versus scaling law (continuous lines). Dimensionless radius is shown as a function of dimensionless scaling time.

**Table 1:** Properties of soils samples, critical stress and Fell erosion index

| Soil         |                              | %      | %    | %     | %          | $\tau_c$ (Pa) | $l_e$ |
|--------------|------------------------------|--------|------|-------|------------|---------------|-------|
|              |                              | Gravel | Sand | Fines | <2 $\mu$ m |               |       |
| Lyell        | silty sand                   | 1      | 70   | 29    | 13         | 8             | 2     |
| Fattorini    | medium plasticity sandy clay | 3      | 22   | 75    | 14         | 6             | 3     |
| Pukaki       | silty sand                   | 10     | 48   | 42    | 13         | 13            | 3     |
| Jindabyne    | Clayey sand                  | 0      | 66   | 34    | 15         | 6 - 72        | 3 - 4 |
| Bradys       | high plasticity sandy clay   | 1      | 24   | 75    | 48         | 50 - 76       | 4     |
| Shellharbour | high plasticity clay         | 1      | 11   | 88    | 77         | 99 - 106      | 4     |
| Waranga      | Low plasticity clay          | 0      | 21   | 79    | 54         | 106           | 4     |
| Matahina     | Low plasticity clay          | 7      | 43   | 50    | 25         | 128           | 4     |
| Hume         | Low plasticity sandy clay    | 0      | 19   | 81    | 51         | 66 - 92       | 4 - 5 |

## Acknowledgement

This research project is sponsored by the French National Research Agency (ERINOH).

## Literature

- [1] Arulanandan, K. and Perry, E.B. 1983. Erosion in relation to filter design criteria in earth dams. *Journal of Geotechnical Engineering*, 109(5), 682-696.
- [2] Bendahmane, F.; Marot, D.; Rosquoët, F.; Alexis, A. 2006. Characterization of internal erosion in sand kaolin soils. *European Journal of Civil Engineering*, 10(4), 505–520.
- [3] Bonelli, S.; Brivois, O.; Borghi, R.; Benahmed, N. 2006. On modelling of piping erosion. *Comptes Rendus de Mécanique*, 8-9(334), 555-559.
- [4] Bonelli, S.; Brivois, O. The scaling law of the hole erosion test with constant pressure drop, *International Journal for Numerical and Analytical Methods in Geomechanics*, to appear.
- [5] Briaud, J.-L. 2006. Chapter 9 - Erosion tests on New Orleans levee samples, in *Investigation of the performance of the New Orleans protection systems in Hurricane Katrina on August 29, 2005. Final report July 31.*
- [6] Dade, W.; Nowell, A.; Jumars, P. 1992. Predicting erosion resistance of muds. *Marine Geology*, 105, 285-297.
- [7] Fell, R.; Fry, J.-J. 2007. *Internal erosion of dams and their foundations*, Taylor & F.
- [8] Graf, W. H. 1984. *Hydraulics of Sediment Transport*. Water Resources publications, LLC.
- [9] Israelachvili, J. N. 1985. *Intermolecular and surface forces*. Academic Press.
- [10] Kenney, T.C.; Lau, D. 1985. Internal stability of granular filters. *Canadian Geotechnical Journal*, 22, 215-225.

- [11] Lefebvre, G.; Rohan, K.; Douville, S. 1985. Erosivity of natural intact structured clay : evaluation, Canadian Geotechnical Journal, 22: 508-517.
- [12] Migniot, C. 1968. A study of the physical properties of different very fine sediment and their behaviour under hydrodynamic action. La Houille Blanche, 7, 591-620.
- [13] Mitchener, H.; Torfs, H. 1996. Erosion of mud/sand mixtures. Coastal Engineering, 29, 1-25.
- [14] Papamichos, E., Vardoulakis, I., Tronvoll, J. and Skjærstein, A. 2001. Volumetric sand production model and experiment. International Journal for Numerical and Analytical Methods in Geomechanics, 25, 789-808.
- [15] Reddi, L.N., Lee, I. and Bonala, M.V.S. 2000. Comparison of internal and surface erosion using flow pump test on a sand-kaolinite mixture. Geotechnical Testing Journal, 23(1), 116-122.
- [16] Saffman, P. 1965. The lift force on a small sphere in a shear flow. Journal of Fluid Mechanics, 22, 385-400.
- [17] Sundborg, A. 1956. The River Klaralven: A study of Fluvial Processes. Esselte Aktiebolag.
- [18] Temple, D.M.; Hanson G.J. 1994. Headcut development in vegetated earth spillways. Applied Engineering in Agriculture. 10(5): 677-682.
- [19] Ternat, F. 2007. Erosion of self-weight consolidated cohesive sediments. Ph-D Thesis, Aix-Marseille II Mediterranean University.
- [20] Wan, C.F.; Fell, R. 2002. Investigation of internal erosion and piping of soils in embankment dams by the slot erosion test and the hole erosion test. UNICIV Report No R-412, The University of New South Wales Sydney ISSN 0077 880X.
- [21] Yalin, M. 1977. Mechanics of Sediment Transport. Pergamon Press.

## **Authors Name and Affiliation**

S. Bonelli

Cemagref, Hydraulics Engineering and Hydrology Research Unit, France  
stephane.bonelli@aix.cemagref.fr

D. Marot

Institute GeM, Interactions Water - Geomaterials Team, France  
didier.marot@iutsn.univ-nantes.fr

F. Ternat

Irphe - CNRS - Universités d'Aix-Marseille, France  
fternat@gmail.com

N. Benahmed

Cemagref, Hydraulics Engineering and Hydrology Research Unit, France  
nadia.benahmed@cemagref.fr